The Astrophysical Journal, 610:851–867, 2004 August 1
© 2004. The American Astronomical Society. All rights reserved. Printed in U.S.A.

COSMIC-RAY ACCELERATION AT RELATIVISTIC SHOCK WAVES WITH A "REALISTIC" MAGNETIC FIELD STRUCTURE

Jacek Niemiec
Instytut Fizyki Jądrowej Polskiej Akademii Nauk, ul. Radzikowskiego 152, 31-342 Kraków, Poland; jacek.niemiec@ifj.edu.pl

and

Michał Ostrowski
Obserwatorium Astronomiczne, Uniwersytet Jagielloński, ul. Orla 171, 30-244 Kraków, Poland
Received 2004 January 20; accepted 2004 April 2

ABSTRACT

The process of cosmic-ray first-order Fermi acceleration at relativistic shock waves is studied with the method of Monte Carlo simulations. The simulations are based on numerical integration of particle equations of motion in a turbulent magnetic field near the shock. In comparison to earlier studies, a few "realistic" features of the magnetic field structure are included. The upstream field consists of a mean field component inclined at some angle to the shock normal with finite-amplitude sinusoidal perturbations imposed upon it. The perturbations are assumed to be static in the local plasma rest frame. Their flat or Kolmogorov spectra are constructed with randomly drawn wavevectors from a wide range ($k_{\rm min}$, $k_{\rm max}$). The downstream field structure is derived from the upstream one as compressed at the shock. We present and discuss particle spectra and angular distributions obtained at mildly relativistic sub- and superluminal shocks. We show that particle spectra diverge from a simple power law; the exact shape of the spectrum depends on both the amplitude of the magnetic field perturbations and the wave power spectrum considered. Features such as spectrum hardening before the cutoff at oblique subluminal shocks and formation of power-law tails at superluminal ones are presented and discussed. The simulations have also been performed for parallel shock waves. The presence of finite-amplitude magnetic field perturbations leads to the formation of locally oblique field configurations at the shock and the respective magnetic field compressions. This results in the modification of the particle acceleration process, introducing some features present in oblique shocks, e.g., particle reflections from the shock. For the first time, we demonstrate for parallel shocks a (nonmonotonic) variation of the accelerated particle spectral index with the turbulence amplitude. At the end, a few astrophysical consequences of the results we obtained are mentioned.

Subject headings: acceleration of particles — cosmic rays — gamma rays: bursts — methods: numerical — relativity — shock waves

1. INTRODUCTION

Relativistic shock waves are postulated to be responsible for a number of phenomena of high-energy astrophysics. Many sources of high-energy radiation appear at the same time to involve highly relativistic plasma flows, indicating that the relativistic shocks are the acceleration sites of energetic particles producing high-energy emission. The observed examples of such flows/shocks can be hot spots in radio galaxies, parsec-scale jets in blazars, jets in Galactic "microquasars," gamma-ray burst sources, and pulsar winds. The understanding of particle acceleration processes at relativistic shocks is essential in the study of these objects.

At relativistic shock waves the bulk flow velocity is comparable to particle velocity. This leads to anisotropy of particle angular distribution, which can substantially influence the process of particle acceleration. The first consistent method to tackle the problem for a parallel shock wave, where the mean magnetic field is parallel to the shock velocity, was proposed by Kirk & Schneider (1987a). Generalizing the diffusive approach by explicit treatment of the particle distribution function anisotropy, they constructed stationary solutions of the pitch-angle diffusion equation on both sides of the shock. The requirement of distribution function continuity at the shock allowed them to match the upstream and downstream solutions by taking into account a sufficient number of high-order terms in particle anisotropy. The solution was obtained from numerical fitting of the respective coefficients. This semianalytic procedure yielded the power-law index of the resulting spectrum, as well as the anisotropic particle angular distribution at the shock. The spectral indices for the phase-space distribution function[1] derived with this method for relativistic shocks—with the compression ratio $R = 4$—were only slightly different from the $\alpha = 4$ value obtained in the nonrelativistic case. These findings were later confirmed by Kirk & Schneider (1987b) with the method of particle Monte Carlo simulations (see also Ellison et al. 1990).

An extension of the above approach was proposed by Heavens & Drury (1988), who modified the method to treat more general conditions at the shock. They investigated the fluid dynamics of relativistic shock waves and applied the results to calculate spectral indices of particles accelerated at such shocks. For a parallel shock wave propagating into cold electron-proton or electron-positron plasma, they found that the particle spectral index depends on the form of the wave power spectrum, in contrast to the nonrelativistic case. The spectral indices obtained were close to the respective values given by the nonrelativistic formula, $\alpha = 3R/(R - 1)$. Kirk &

[1] The energy spectral index of the particle distribution function $N(E) \propto E^{-\sigma}$, often used in the gamma-ray burst studies, is $\sigma = \alpha - 2$.

Heavens (1989) considered the acceleration processes in shocks with magnetic fields oblique to the shock normal. For the subluminal shock configurations studied they assumed magnetic moment conservation for particles interacting with the shock. This assumption restricted the validity of their considerations to the case of a weakly perturbed magnetic field. The important result of this work was that oblique shocks lead to flatter spectra than parallel ones; a spectrum could be even as flat as $\alpha \approx 3$ in cases where the shock velocity along magnetic field lines is close to the speed of light. This feature arises because of effective multiple reflections of anisotropically distributed upstream particles from the compressed downstream magnetic field. However, as pointed out by Begelman & Kirk (1990), most field configurations in relativistic shocks lead to superluminal conditions for the acceleration process. Therefore, unless there is strong particle scattering across field lines, particles are not able to cross the shock front repeatedly and diffusive acceleration is inefficient. Instead, particle energy gains are due to the shock-drift acceleration process, which involves a single shock transmission of upstream particles downstream of the shock (Webb et al. 1983; Drury 1983).

The above approximations rely on an assumption of a weakly perturbed magnetic field, where cross-field diffusion does not play a significant role. However, in astrophysical shocks one may expect large-amplitude MHD waves to occur. In such conditions, scattering of particles is not exclusively related to resonant interactions with the magnetic field fluctuations, as in the small-amplitude wave limit. In this case, the Fokker-Planck equation does not properly describe the particle transport, nor does the particle magnetic moment conservation hold for oblique shocks (Decker & Vlahos 1985; Ostrowski 1991). Thus, the particle acceleration process has to be investigated with the help of numerical methods.

The role of finite-amplitude magnetic field perturbations in forming a particle spectrum was investigated by a number of authors using Monte Carlo particle simulations (e.g., Ellison et al. 1990; Ostrowski 1991, 1993; Ballard & Heavens 1992; Naito & Takahara 1995; Bednarz & Ostrowski 1996, 1998). The main result of these considerations was the finding of a direct dependence of the derived particle spectra on the conditions near the shock. The power-law spectra can be either very steep or very flat for different mean magnetic field inclinations to the shock normal and different amplitudes of perturbations, where changes of the particle spectral index can be nonmonotonic with an increasing field perturbations amplitude (Ostrowski 1991, 1993).

The process of the first-order Fermi acceleration at ultrarelativistic shocks ($\gamma \gg 1$) has been studied in the last few years by a number of authors (Bednarz & Ostrowski 1998; Gallant & Achterberg 1999; Gallant et al. 1999; Achterberg et al. 2001; Kirk et al. 2000; Lemoine & Pelletier 2003). All these approaches yield consistent estimates of the asymptotic ($\gamma \rightarrow \infty$) spectral index $\alpha \approx 4.2$–4.3 in the limit of highly turbulent conditions near the shock (see Ostrowski & Bednarz 2002). In conditions with medium-amplitude magnetic field perturbations, the particle spectra generated at ultrarelativistic shocks can be much steeper than those obtained in the asymptotic limit, as seen in the simulations of Bednarz & Ostrowski (1998).

Numerical investigations of the first-order Fermi process are based on simulations of particle motion in a turbulent magnetic field near the shock front. One possible method is to use the pitch-angle diffusion model to study particle transport in a way similar to the quasi-linear analytic approximation. Such an approach was first presented by Kirk & Schneider (1987b), and essentially the same technique was independently elaborated for oblique shocks by Ostrowski (1991; see also Bednarz & Ostrowski 1996, 1998). In this approach, a particle is assumed to move in a regular magnetic field along its undisturbed "adiabatic" trajectory, and the influence of the turbulent field on the orbit is described by discrete, uncorrelated, small-amplitude particle pitch-angle perturbations in finite time intervals. Depending on the model parameters—the mean time between successive scattering acts and the scattering amplitude—one is able to simulate situations with different magnetic field configurations and different turbulence amplitudes.

The other and perhaps more basic method of numerical simulations is to specify the entire magnetic field in the space near the shock and to integrate particle equations of motion in such a "realistic" field. However, this method is much more difficult to implement because precise numerical calculations of particle trajectories in a wide wavevector range spectrum require usually excessive simulation times. Because of this fact, the two early papers adopting this technique for relativistic shock waves had to apply very simple models of a turbulent magnetic field. Ballard & Heavens (1992) considered a highly disordered magnetic field with vanishing regular component, equivalent to discussing a parallel highly turbulent shock. The field was described in Fourier space by the Kolmogorov power-law spectrum in a very limited wavevector range, $k_{\max}/k_{\min} \approx 20$. In their approach, the upstream and downstream turbulent fields were unrelated and, in addition, a new turbulent field pattern was selected at each particle shock crossing. Because of the restricted dynamical range for the magnetic field perturbations, the resulting particle spectra were formed in a limited energy range near the injection energy. A different approach was presented by Ostrowski (1993). In his work, the magnetic field consisted of the regular component and the perturbations, described as the superposition of a few sinusoidal static waves of finite amplitude, oriented randomly with respect to the mean field. For each particle of a given energy there were three wavevector ranges, containing short, resonance, and long waves with the flat power spectrum. When in the course of the acceleration process a particle energy increased, the respective short waves were replaced by the existing previously resonance wavevectors, the resonance waves by the long ones, and a new set of waves was selected for the long waves. With this procedure, one was able to study particle acceleration to very high energies, which allowed for an accurate determination of the spectral indices in an energy range not influenced by the initial conditions. The spectra obtained by Ostrowski for parallel shocks were systematically flatter than those calculated by Ballard & Heavens (1992; see discussion in Ostrowski 1993).

The purpose of our present work is to simulate the first-order Fermi acceleration process at (mildly) relativistic shock waves, propagating in more realistically modeled perturbed magnetic fields. This involves the use of a wide wavevector range turbulence with a power-law spectrum and continuity of the magnetic field across the shock front, according to the respective matching conditions. Particle trajectories are calculated by integrating their equations of motion in such fields. Both sub- and superluminal mean magnetic field configurations are studied, as well as the particular case of parallel

shocks. Angular distributions and wide-energy particle spectra are derived in a range of model parameters. We show that the particle spectra diverge from a simple power law in the full energy range considered, yielding in some cases interesting spectral features. A number of previously obtained results are also reproduced. The simulation method and the magnetic field structure assumed are described below, in § 2. The results are presented in § 3 and finally summarized and discussed in § 4.

Below, the speed of light c is used as the velocity unit. All calculations are performed in the respective local plasma (upstream or downstream) rest frames. The upstream and downstream quantities are labeled with the indices 1 and 2, respectively. We consider ultrarelativistic particles with $p = E$. In the units we use in our simulations, a particle of unit energy moving in a uniform mean upstream magnetic field $B_{0,1}$ has the unit maximum (for $p_\perp = E$) gyroradius $r_g(E = 1) = 1$ and the respective resonance wavevector $k_{\rm res}(E = 1) = 2\pi$.

2. SIMULATIONS

In our simulations, trajectories of ultrarelativistic test particles are derived by integrating their equations of motion in a perturbed magnetic field. A relativistic shock wave is considered to be a planar discontinuity, propagating in a rarefied (collisionless) electron-proton plasma with a turbulent magnetic field frozen in it. Upstream of the shock, the field is assumed to consist of the uniform component $\boldsymbol{B}_{0,1}$, inclined at some angle ψ_1 to the shock normal, with finite-amplitude perturbations imposed upon it. The irregular component has either a flat $[F(k) \sim k^{-1}]$ or a Kolmogorov $[F(k) \sim k^{-5/3}]$ wave power spectrum in the (wide) wavevector range ($k_{\rm min}$, $k_{\rm max}$). The perturbations are assumed to be static in the local plasma rest frame, both upstream and downstream of the shock. Thus, the possibility of second-order Fermi acceleration is excluded from our considerations. The shock propagates with velocity u_1 with respect to the upstream plasma. The magnetic field is assumed to be dynamically unimportant, and its downstream structure, together with the downstream flow velocity u_2, is obtained from hydrodynamic jump conditions for shocks propagating in the cold electron-proton plasma. Derivation of the shock compression ratio, defined in the shock rest frame as $R = u_1/u_2$, is based on the approximate formulae derived by Heavens & Drury (1988). For the case of the shock propagating with velocity $u_1 = 0.5c$ studied in this paper, these formulae give $R \simeq 5.11$. For the shock velocity $u_1 = 0.9c$, the shock compression ratio is $R \simeq 3.92$, and for $u_1 = 0.98c$, $R \simeq 3.29$. The acceleration process is considered in the particle energy range where radiative (and other) losses can be neglected.

The model of the medium near the shock used in the paper is constructed by four elements: the turbulent magnetic fields upstream and downstream of the shock and the two free escape boundaries, located far upstream and far downstream from the shock front. The magnetic field structure is described below in § 2.1, and the cause for introducing the boundaries is explained in § 2.2.

2.1. *Magnetic Field Structure*

The "turbulent" (≡perturbed) magnetic field component upstream of the shock is modeled as a superposition of sinusoidal static waves of finite amplitude (see Ostrowski 1993). In our simulations, in a magnetic field–related primed coordinate system,[2] they take the form

$$\delta B_{x'} = \sum_{l=1}^{294} \delta B_{x'l} \sin\left(k^l_{x'y'} y' + k^l_{x'z'} z'\right), \tag{1}$$

where $(k^l_{x'y'})^2 + (k^l_{x'z'})^2 = (k^l_{x'})^2$ (see below), and analogously for $\delta B_{y'}$ and $\delta B_{z'}$ components. Such a form of $\delta \boldsymbol{B}$ ensures that $\nabla \cdot \boldsymbol{B} = 0$. The index l enumerates the wavevector range from which the wavevectors $k^l_i (i = x', y', z')$ are randomly drawn. The components $k^l_{x'y'}$, $k^l_{x'z'}$ of the wavevectors $k^l_{x'}$ are selected by choosing a random phase angle $\phi^l_{x'}$, so that $k^l_{x'y'} = k^l_{x'} \cos \phi^l_{x'}$ and $k^l_{x'z'} = k^l_{x'} \sin \phi^l_{x'}$, and analogously for other components. The wavevectors span the range ($k_{\rm min}$, $k_{\rm max}$), where $k_{\rm min} = 0.0001$ and $k_{\rm max} = 10$. The selected form of the perturbations and the method of k^l_i vector component drawing both produce isotropic turbulence. The number of 294 wavevector ranges used in the simulations has been selected on the basis of a series of numerical tests. It has been checked that this number is sufficient for the perturbed magnetic field to diffusively scatter particles. Using a larger number of waves would result in longer simulation times. On the other hand, taking a substantially smaller number of waves could lead to resonance (nonstochastic) features in the particle trajectories (see Karimabadi et al. 1992).

The wave amplitudes δB_{il} are selected at random to satisfy $\delta B^2_l = \sum_i \delta B^2_{il}$, and the amplitudes δB_l are chosen to reproduce the turbulence power spectrum assumed. In the wavevector range considered, this spectrum can be written

$$\delta B_l(k) = \delta B_l(k_{\rm min}) \left(\frac{k}{k_{\rm min}}\right)^{(1-q)/2}, \tag{2}$$

where q is the wave spectral index; $q = 1$ corresponds to the flat spectrum and $q = 5/3$ to the Kolmogorov one. The constant $\delta B_l(k_{\rm min})$ is scaled to match the model parameter $\delta B \equiv (\sum_l \delta B^2_l)^{1/2}$. Its ratio to the upstream mean magnetic field, $\delta B/B_{0,1}$, is our measure of the field perturbation amplitude.

The Kolmogorov wave power spectrum $F(k) \sim k^{-5/3}$ $[\delta B^2 = \int F(k) dk]$ seems to be an appropriate (although still approximate) choice for magnetic field turbulence description in real astrophysical plasmas. Such a spectrum is measured in the solar wind (Leamon et al. 1998). Interstellar scintillation observations indicate that the electron density spectrum follows the Kolmogorov slope (Lee & Jokipii 1976; Lagage & Cesarsky 1983; Cho 2001; Stinebring et al. 2000; see, however, Boldyrev et al. 2002), and the same character could probably be ascribed to the MHD turbulence power spectrum (Cho 2001; Cho et al. 2003). Such a form of the spectrum of perturbations was also often used in modeling of acceleration processes at shocks. The flat turbulence power spectrum, $F(k) \sim k^{-1}$, is considered here in order to check how the accelerated particle spectra depend on the value of the wave spectral index and also to compare our results to the earlier studies. The simulations are performed for the case of a

[2] In the upstream plasma rest frame the x-axis of the (unprimed) Cartesian coordinate system (x, y, z) is perpendicular to the shock surface. The shock wave moves in the negative x-direction, and the regular magnetic field lies in the x-y plane. The primed system (x', y', z') is obtained from the unprimed one by its rotation about the z-axis by an angle ψ_1, so that the x'-axis is directed along $\boldsymbol{B}_{0,1}$.

weakly ($\delta B/B_{0,1} \ll 1$) and a highly ($\delta B/B_{0,1} \gtrsim 1$) perturbed magnetic field. The finite-amplitude magnetic field perturbations can exist in the plasma where the shock wave propagates, as observed, e.g., for heliospheric plasma, where $\delta B/B_{0,1} \sim 1$ (see Ellison et al. 1990). Calculations for nonrelativistic shocks indicate that the turbulence can be also produced upstream of the shock by nonlinear interactions between MHD waves generated by accelerated particles (Drury 1983; Lagage & Cesarsky 1983; Lucek & Bell 2000). In such a case, the resulting form of the turbulence spectrum is not satisfactorily known.

The downstream magnetic field structure is obtained from the upstream one as compressed at the shock. According to the gas compression conditions, any given point (x_2, y, z) in the downstream plasma was at the position $(x_1 = rx_2, y, z)$ in the upstream rest frame before the shock passage. One should note that the upstream and the downstream magnetic fields are compared in two time instants, before and after the shock passage, respectively. The compression factor $r = R\gamma_1/\gamma_2$, where R is the shock compression ratio in the shock-normal rest frame and $\gamma_i = 1/(1 - u_i^2)^{1/2}$ $(i = 1, 2)$. Thus, to derive the downstream field components at the point (x_2, y, z) we calculate the unshocked magnetic field at the point (x_1, y, z) and compress the tangential components of the magnetic field by the factor r. The field component parallel to the shock normal remains unchanged. Note that the magnetic field derived in such a way is continuous across the shock. In our approach, the shock front itself does not produce any additional fluctuations of the field. However, as pointed out by Medvedev & Loeb (1999; see also Nishikawa et al. 2003; Frederiksen et al. 2003, 2004) the relativistic two-stream instability can generate small-scale strong magnetic field perturbations in the vicinity of the shock. Thus, our modeling can be considered valid only for high-energy particles, with gyroradii much larger than the spatial scale of inhomogeneities thus generated. A study of the influence these small-scale perturbations have on the particle spectra formation is planned in future work.

2.2. *Simulation Method*

The particle equations of motion are integrated in the local (upstream or downstream) plasma rest frame, where the electric field vanishes. At the beginning of the simulation run, N monoenergetic particles (usually $N = 100$) are injected at the shock front with their momentum vectors directed into the upstream region. Particle injection energy measured in the downstream rest frame is $E_0 = 0.1$ and their resonance wavevectors $k_{\rm res}(E_0) \gg k_{\rm max}$.[3] After the Lorentz transformation to the upstream plasma rest frame, the trajectory of each particle is followed until it crosses the shock surface or reaches an introduced free escape boundary, located far upstream from the shock. In the latter case, the particle is assumed to escape from the acceleration region. The boundary is required to treat high-energy particles, with resonance wavevectors much smaller than $k_{\rm min}$, but also the low-energy particles, with $k_{\rm res} \gg k_{\rm max}$.[4] Such particles are only weakly scattered by the turbulent field and can propagate very far upstream from the shock. The upstream particles that cross the shock front are Lorentz-transformed into the downstream plasma rest frame. At this side of the shock a free escape boundary is located "far downstream" from the shock at $x_{\rm max}(E) = X_{\rm max} r_g(E)$ behind it. The selected value of the coefficient $X_{\rm max} \in (5, 150)$ depends on simulation parameters and is specified by numerical tests, separately for each shock configuration. In the conditions considered by us, very few particles are able to diffuse from such a distance back to the shock. The trajectory of a particle downstream of the shock is integrated until it crosses the escape boundary or reaches the shock front. After performing this procedure for all N particles, the first simulation cycle is finished. Then the splitting procedure is performed (see below) to replace all escaped particles with the ones still active in the acceleration process, with the respective division of the particle weights. Subsequent cycles' calculations are performed analogously. The computations are finished when either more than 90% of particles escape through the introduced boundaries in an individual simulation cycle or all particles reach the upper energy boundary $E_{\rm max} = 10^8$ or the lower limit for a particle weight $w_{\rm min}$ (see below), which is usually set to $10^{-6} w_0$. We have checked that allowing for further calculations does not noticeably influence the spectrum formed.

We use the method of trajectory splitting to derive spectra in a wide energy range. This method is a standard tool of Monte Carlo particle simulations (e.g., Hammersley & Handscomb 1965; see also Kirk & Schneider 1987b; Ostrowski 1991, 1993). At the beginning of the simulations, the same initial weight w_0 is ascribed to each particle. During the calculations, some particles are lost by escaping through the boundaries. To keep the total number of particles active in the simulations constant, for each lost particle we duplicate (or "multiplicate") one of those that crossed the shock upstream, with the weight of the original particle divided at equal parts between the "daughter" particles. Then we weakly perturb the motion of these particles to create different trajectories out of the split one. The perturbations are performed by a small change in particle positions in the shock plane, $\Delta y, \Delta z \sim 0.0002 \lambda_{\rm min}(E)$, where $\lambda_{\rm min}(E)$ is the smallest scale of the resonant range of the field perturbations, defined in § 2.3. For the splitting procedure we take particles with the highest weights and smallest energies available. With this method, the effective number of particles in the simulation is much higher than the injected number, and a particle spectrum is determined with approximately the same accuracy at all energies.

A spectrum of accelerated particles and their angular distribution are measured at the shock, in the shock rest frame. Every time a particle crosses the shock front, a value $w/(|v_x| + 0.005)$ is added to the respective logarithmic energy bin and to the

[3] For superluminal shocks the seed particle injection procedure is modified. In this case, the majority of injected particles escape downstream after the first interaction with the shock and only a few particles are still able to take part in the acceleration process. The resulting spectra are then determined with poor accuracy. To overcome this problem, we increase the number of injected particles in such a way as to select N of those that, after transmission downstream, succeed in reaching the shock front again. We have checked that this method gives the same results when applied to subluminal shocks; the only difference appears at the energy range close to E_0, which is already influenced by the initial conditions.

[4] The upstream escape boundary for low-energy particles with $k_{\rm res} \gg k_{\rm max}$ is introduced only in the case of oblique subluminal and parallel shock waves, propagating with velocity $u_1 = 0.5c$ in the weakly perturbed magnetic field ($\delta B/B_{0,1} = 0.3$). In these cases, the upstream boundary is located at several tens of thousands of r_g ahead of the shock front. The escape boundary for energetic particles ($k_{\rm res} \ll k_{\rm min}$) is located at $200 r_g(E)$ ahead of the shock in the case of oblique subluminal shocks, whereas for parallel shocks it is placed at $2000 r_g$ upstream of the shock. The number of low-energy particles escaping upstream is small. However, for the highest energy particles, with $k_{\rm res}(E) \ll k_{\rm min}$, the escape becomes efficient, leading to the formation of the cutoff in particle spectra.

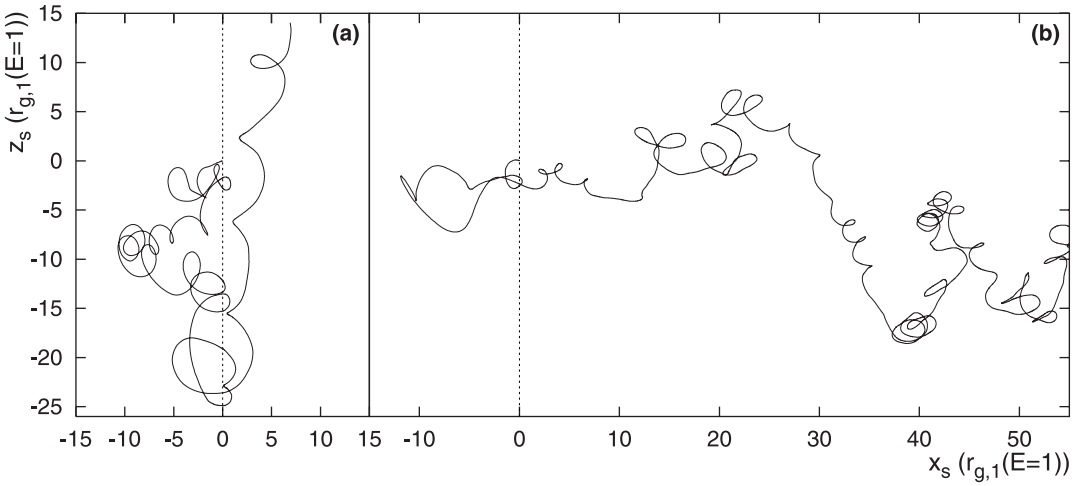


FIG. 1.—Example particle trajectories projected onto the x_s-z_s plane in the shock-normal rest frame. The trajectories were calculated for particles of initial energy $E_1 = 1$, injected at the shock with different initial conditions (a momentum inclination to the shock normal, the magnetic field strength and inclination at the injection point) and shock parameters $u_1 = 0.5c$, $\psi_1 = 45^\circ$, and $\delta B/B_{0,1} = 1.0$. The shock front is shown by a dotted line and the trajectories originate at (0, 0). The effects of the turbulent magnetic field structure, including the presence of long-wave perturbations, are visible in the figure. The particle in (*a*) crosses the shock front several times and is accelerated up to $E_2 \approx 11.8$. The particle in (*b*) is accelerated up to $E_2 \approx 3.3$ and then escapes far downstream from the shock.

respective $\cos\theta$ bin. Here θ is the angle between the particle momentum and the shock normal (note that θ is not the pitch angle measured with respect to the mean magnetic field), v_x is a normal component of the particle velocity, and w is its weight. The weighting factor ($|v_x| + 0.005$) is needed to transform the particle flux into the particle density (see Kirk & Schneider 1987b), and the additional term 0.005 ensures proper behavior near $v_x = 0$. The spectra and angular distributions presented are averaged ones over a few (usually 10) different sets of N particles and realizations of the perturbed magnetic field.

2.3. *Derivation of Particle Trajectories*

The particle orbits are calculated using the Runge-Kutta fifth-order method with the adaptive step size control (routine RKQS in Press et al. 1992). This routine allows for an accurate derivation of particle trajectories in a turbulent magnetic field with the optimized simulation time (see also Appendix B). However, the procedure becomes very time consuming for higher energy particles because exact derivation of a trajectory with short-wave perturbations requires extremely short time steps (in units of r_g/c) to be used. At the same time, the considered short waves, with $\lambda \ll r_g$, only weakly influence trajectories of such particles. Therefore, in our modeling the motion of a higher energy particle is derived within the proposed hybrid approach. It involves exact integration of particle trajectories in the turbulent field including long and resonance waves [$\lambda > \lambda_{\min} = 0.05 r_g(B = B_{0,1})$],[5] and the short-wave influence on the trajectory is included as a respective small-amplitude momentum scattering term. A scattering probability distribution is determined by additional simulations, involving the full set of the short waves considered (see Appendix A). Example particle trajectories are shown in Figure 1.

2.4. *Tests*

A number of tests have been performed on the simulation code. Some of them have been mentioned in the preceding subsections; the others are described in detail in Appendix B.

[5] The short waves downstream of the shock are defined by a particle gyroradius in the upstream mean magnetic field $B_{0,1}$. However, this assumption does not influence the particle spectra formed, as discussed in Appendix B.

3. RESULTS

Our Monte Carlo simulations of the first-order Fermi acceleration process have been performed in order to study the role of the applied magnetic field structures for the test particle acceleration at relativistic shocks. Because of the limited dynamic range of field perturbations, scattering conditions vary with increasing particle energies. We study how this influences the particle spectrum formation and how the spectra depend on the shock velocity and on the parameters of the magnetic field: the mean field inclination and the spectrum of finite-amplitude perturbations. In the case of oblique subluminal shocks, the accelerated particle spectral index can vary with the turbulence amplitude. At superluminal shocks, the presence of finite-amplitude perturbations near the shock plays an essential role in particle acceleration. In weakly scattering conditions, the first-order Fermi process is inefficient in such shocks and particles can gain energies only from the one-way compression at the shock (Begelman & Kirk 1990). Formation of power-law spectra is possible for larger amplitudes of the magnetic field perturbations. In particular, we discuss the role of long-wave perturbations, which lead to the formation of locally oblique subluminal configurations at the shock. In the conditions provided, the energy gains of particles interacting with the shock can increase and particle reflections from the respective regions of the compressed field downstream of the shock may occur. The importance of this factor on particle spectra formation is investigated for parallel shocks as well.

Accelerated particle spectra formed at oblique shock waves are presented in Figure 2 for the case of subluminal magnetic field configuration and in Figures 5 and 9 for superluminal shocks. Particle spectra derived for parallel shocks are shown in Figure 10. The particle spectra were calculated for three different upstream magnetic field perturbation amplitudes $\delta B/B_{0,1} = 0.3$, 1.0, and 3.0, referred to below as the small, medium, and large (high) amplitude perturbations, respectively. The amplitudes $\delta B/B_{0,1}$ are indicated in the figures near

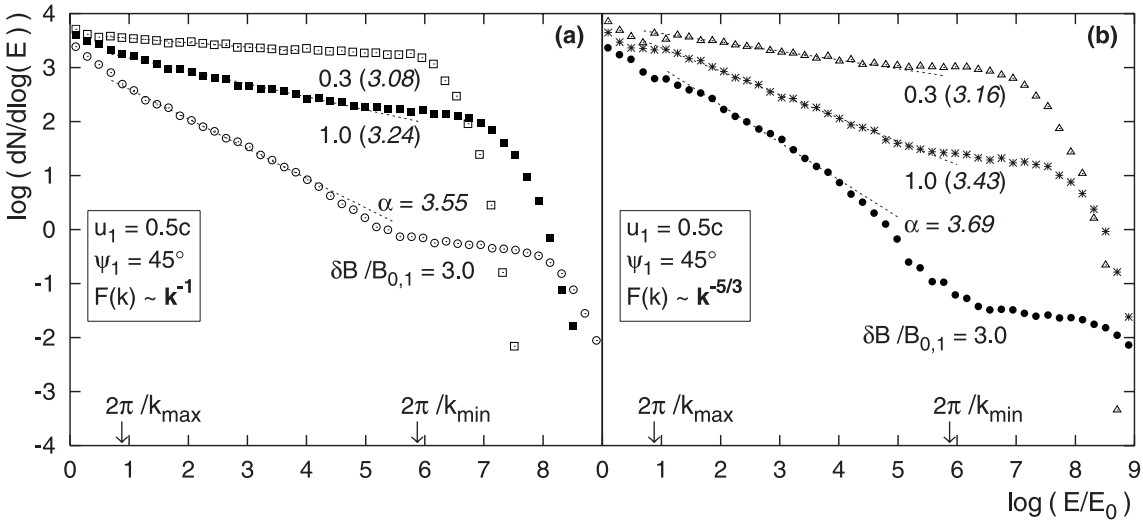


FIG. 2.—Particle spectra at the subluminal shock wave ($u_1 = 0.5c$, $\psi_1 = 45^\circ$, and $u_{B,1} \simeq 0.71c$) for (*a*) the flat and (*b*) the Kolmogorov wave spectrum of magnetic field perturbations. Any individual point in the spectrum represents a particle number (weight) dN recorded per a logarithmic energy bin. The upstream perturbation amplitude $\delta B/B_{0,1}$ is given near the respective results. Linear fits to the spectra are also presented and values of the spectral indices α are given in italic. The spectra have vertical shifts for clarity. Particles with energies in the range $(2\pi/k_{\max},\ 2\pi/k_{\min})$ indicated by arrows can effectively interact with the magnetic field inhomogeneities.

the respective curves. Spectra for different $\delta B/B_{0,1}$ are not normalized; they have vertical shifts for presentation clarity. Linear fits to the power-law parts of the spectra are also presented in the figures, and values of the spectral indices α are given. Accuracies of the presented fits are usually better than 0.02 in α for subluminal and parallel shocks, with some exceptions discussed in the following. For superluminal shocks, the evaluated statistical errors $\Delta\alpha \approx 0.03-0.06$. One should note that the power-law character of some particle spectra is only approximate because of the existing spectrum curvature (see, e.g., Figs. 5*d*, 5*f*, and 9*b*) and thus that the value of the spectral index derived depends also directly on an energy range chosen for the fit. The narrow energy range values of α, indicated in Figures 5 and 9, are shown for comparison to the spectral indices of the other spectra presented.

Particles in the energy range indicated in the figures by arrows above the horizontal energy axis can effectively interact with the magnetic field inhomogeneities because of the resonant condition satisfied, $k_{\min} \lesssim k_{\rm res} \lesssim k_{\max}$ ($k_{\rm res} \equiv 2\pi/r_g$). The limits are not precise; they are calculated for the upstream magnetic field strength $B_{0,1} = 1$ and particle transverse momenta $p_\perp = p$. The particle energies considered in the simulations can be scaled to various shock conditions by the respective identifications of $B_{0,1}$, ψ_1, δB, $k_{\min}$, and $k_{\max}$.

3.1. *Oblique Subluminal Shock Waves*

To illustrate the characteristic features of particle acceleration processes at relativistic oblique subluminal ($u_1/\cos\psi_1 < c$) shocks, we have studied the shock wave propagating with velocity $u_1 = 0.5c$ ($\gamma_1 \simeq 1.2$) into the upstream plasma with the mean magnetic field inclined to the shock normal at $\psi_1 = 45^\circ$. The shock velocity along the mean magnetic field is then $u_{B,1} \simeq 0.71c$. Figure 2 shows accelerated particle spectra, derived in the shock rest frame, for the flat and the Kolmogorov wave power spectrum. One may note that the particle spectra diverge from a power law in the full energy range. Usually a harder spectral component appears at the highest energies, followed by the spectrum cutoff. The shape of the particle spectrum depends on both the amplitude of the magnetic field perturbations and the spectral index of the wave power spectrum.

The power-law part of the particle spectrum steepens with the increasing amplitude of the field perturbations for the three cases considered. For the flat turbulence spectrum, the particle spectrum is very flat ($\alpha \approx 3.08$) for the weakly perturbed field $\delta B/B_{0,1} = 0.3$. For larger perturbation amplitudes we have $\alpha \approx 3.24$ and $\alpha \approx 3.55$ for $\delta B/B_{0,1} = 1.0$ and 3.0, respectively. The spectral indices obtained are consistent with previous numerical calculations of Ostrowski (1991, 1993) and, in the limit of small perturbations, with the analytic results obtained by Kirk & Heavens (1989).

Variations of the accelerated particle spectral index with the turbulence amplitude, for a given mean field inclination, was discussed by Ostrowski (1991). As already mentioned in § 1, in a weakly perturbed magnetic field there is a high probability of reflection of upstream particles from the compressed field behind the shock. The repeating particle reflections lead to the formation of a very flat energy spectrum. When the perturbation amplitude increases, the reflection probability is diminished and the mean energy gains of particles interacting with the shock decrease. At the same time, the escape probability for downstream particles decreases, since the field perturbations enable particles to diffuse across the field lines. However, this reduction of the escape probability is slow, so that increased upstream-downstream transmission probability leads to a net more efficient particle escape and the resulting steepening of the spectrum.

The differences in the particle spectra obtained for the Kolmogorov and the flat wave power spectrum are clearly visible from comparison of Figures 2*a* and 2*b*. In particular, for a given $\delta B/B_{0,1}$ the power-law part of the spectrum is steeper for the Kolmogorov wave spectrum, and the final hardenings of the spectra are more pronounced in this case.

The non–power-law character of the obtained particle spectra results from the limited dynamic range of the magnetic field perturbations. In the energy range where an approximate power-law spectrum forms, particles are effectively scattered by the resonant magnetic field inhomogeneities. The character

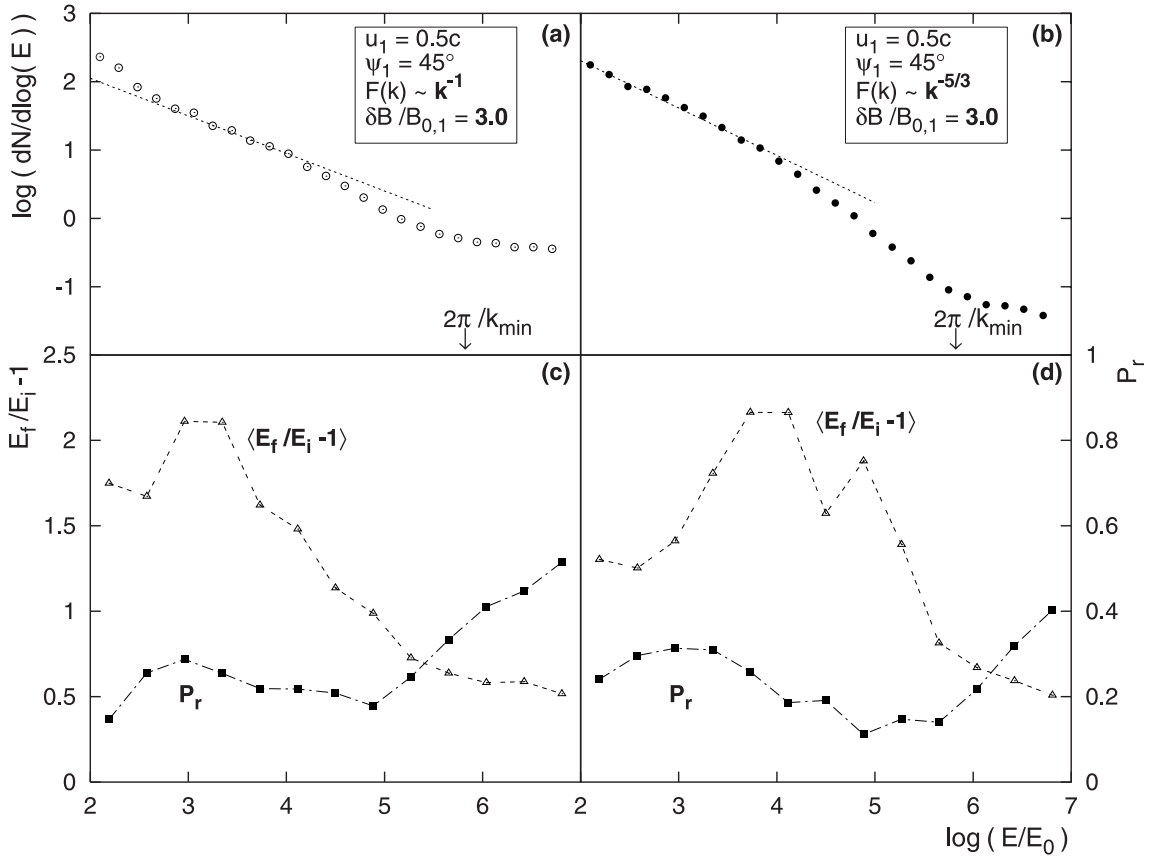


FIG. 3.—Probability of particle reflection P_r and the mean energy gain of reflected particles $\langle E_f/E_i - 1\rangle$ in the energy range where the particle spectrum deviates from a power-law form. The respective parts of particle spectra are shown in the top panels. Power-law fits are the same as shown in Fig. 2. The values of P_r and $\langle E_f/E_i - 1\rangle$ were obtained in additional simulations, with the particle injection energy $E = 10$, so that the first few points are influenced by the initial conditions. In this figure, the energies E_i and E_f are measured in the upstream plasma rest frame and the particle spectra are also calculated in this frame. To limit statistical fluctuations, the logarithmic energy bin used in the bottom panels is twice as large as the respective bins in the top panels. The respective upstream-downstream transmission probability $P_{12} = 1 - P_r$.

of the spectrum changes at high particle energies, for which resonance wavevectors $k_{\rm res} \lesssim k_{\rm min}$. These particles interact with the magnetic field perturbations being the short-wave turbulence and are only weakly scattered. Thus, analogously to weakly scattering conditions, the anisotropically distributed upstream particles can be effectively reflected from the region of the compressed magnetic field downstream of the shock, leading to the spectrum flattening. The effectiveness of reflections and the resulting modification of the spectrum depend on the amplitude and the spectrum of field perturbations, as can be seen in the figures. Finally, a cutoff in the spectrum appears because of weakly scattered particles escaping through the introduced upstream boundary.

Effects of the finite wavevector range can also be observed for particles within the resonance range $k_{\rm min} \lesssim k_{\rm res} \lesssim k_{\rm max}$ for the magnetic field perturbations considered. The change of the scattering conditions with the increasing particle energies should lead to the modest but continuous variation of the particle spectral slope. The effect is visible (Fig. 3) for the case of a highly turbulent magnetic field $\delta B/B_{0,1} = 3.0$. The noticeable steepening of the spectrum for particle energies $\log(E/E_0) \gtrsim 4$ is accompanied by a slow decrease of the probability of reflection, P_r, and the mean energy gain at an individual particle-shock interaction (Figs. 3*c* and 3*d*; for the probability of reflection and the mean energy gains calculations, see § 3.4). At higher energies, P_r starts to grow again, without any increase in $\langle E_f/E_i - 1\rangle$, which results in a harder spectrum. Thus, the main factor leading to the variation of a spectrum inclination is the increased upstream particle transmission probability and thus the increased escape probability. The decrease in P_r and in the mean energy gain of reflected particles stems possibly from the fact that for high-energy particles (but still with $k_{\rm res} \gtrsim k_{\rm min}$) there are gradually fewer large-amplitude long-wave magnetic field perturbations for an increasing particle energy and, therefore, the effective mean inclination of the magnetic field at the shock decreases, leading to the effects discussed. These effects are not visible in the spectra for smaller $\delta B/B_{0,1}$ since the amplitudes of long-wave perturbations are moderate in these cases. In the case of the Kolmogorov wave power spectrum yet other effects might be responsible for the decrease in the reflection probability. The first factor is related to the increasing amplitude of the resonant perturbations with the increasing particle energy, leading to a gradual breakdown of approximate magnetic moment conservation. At the same time, the perturbation amplitude growth leads to additional isotropization of particles hitting the shock from upstream. This increases the mean inclination of particle momenta crossing the shock, increasing the mean energy gain of a few reflected particles, and increases the particle upstream-downstream transmission probability (see Ostrowski 2002). The effect can be also visible for particles forming the power-law part of the spectrum. As Figures 3*b* and 3*d* show, the mean energy gain grows with energy for these particles, the feature not observed with the flat wave power spectrum (Figs. 3*a* and 3*c*).

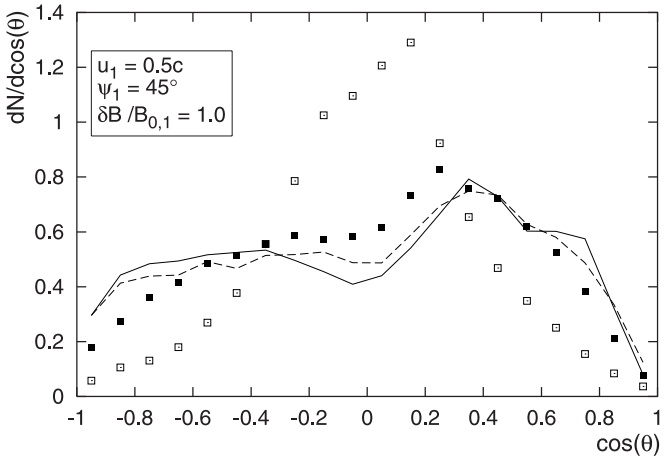


FIG. 4.—Particle angular distributions at the shock front for $\delta B/B_{0,1} = 1.0$ in the shock rest frame. The angular distributions for particles forming the power-law part of the energy spectrum, $1 \leq \log(E/E_0) \leq 5$, are shown by the filled and open squares for the flat and the Kolmogorov wave power spectrum, respectively. Angular distributions for particles responsible for the harder spectral component, $5 \leq \log(E/E_0) \leq 7$, are presented by the solid (flat spectrum) and dashed (Kolmogorov spectrum) lines. All distributions are normalized to the unit surface area under the respective curves. Particles with $\cos\theta < 0$ are directed upstream of the shock.

Example particle angular distributions at the shock are presented in Figure 4 for particles forming the power-law part of the energy spectrum and for particles responsible for the flatter high-energy spectral component. Anisotropies of the distributions presented for the power-law parts of the particle spectra are larger in the case of the Kolmogorov wave power spectrum. Angular distributions for particles forming the harder spectral component hardly depend on the wave power spectrum.

3.2. *Oblique Superluminal Shock Waves*

Spectra for superluminal shocks are presented in Figure 5 for a number of the mean magnetic field configurations and shock velocities (Lorentz factors) $u_1 = 0.5c$ ($\gamma_1 \simeq 1.2$) and $u_1 = 0.9c$ ($\gamma_1 \simeq 2.3$). For the inclination angle $\psi_1 = 75^\circ$ considered, the shock wave propagation velocity along the mean magnetic field component is $u_{B,1} \simeq 1.93c$ for $u_1 = 0.5c$ and $u_{B,1} \simeq 3.48c$ for $u_1 = 0.9c$. For the smaller $\psi_1 = 45^\circ$ and the shock velocity $u_1 = 0.9c$, the projected velocity $u_{B,1} \simeq 1.27c$.

For the small turbulence amplitude ($\delta B/B_{0,1} = 0.3$) in all cases studied, we approximately reproduce the results of Begelman & Kirk (1990), showing a "superadiabatic" compression of injected particles but hardly any or an extremely steep power-law spectral tail. However, our method of particle injection does not match initial conditions of the compression process, which takes place when the initially isotropically distributed particles cross the shock. Because of this, in order to directly estimate the role of this process on particle spectrum formation, additional simulations have been performed. In these simulations, a set of $N = 20,000$ particles with energy $E_{0,1} = E_0$ was injected $10r_{g,1}$ in front of the shock with the isotropic angular distribution in the upstream plasma rest frame. In these simulations we studied a shock wave propagating with velocity $u_1 = 0.5c$ in the plasma with the magnetic field composed of the regular component only ($\delta B/B_{0,1} \equiv 0$) inclined at an angle $\psi_1 = 45^\circ$ to the shock normal (see Figs. 5*a* and 5*b*). Therefore, in the absence of scattering, the particle energy gains are solely due to the acceleration at individual shock transmissions. The trajectory of each injected particle was followed until, after interacting with the shock surface, it reached the free escape boundary located $30r_{g,2}$ downstream of the shock. Note that an interaction with the shock wave may involve a number of particle trajectory crossings of the shock front. The resulting particle spectrum is shown in Figure 6 (*filled squares*), where the spectra formed in the weakly perturbed magnetic field $\delta B/B_{0,1} = 0.3$ are also presented for comparison. These spectra were calculated using the above-described method, with particle injection upstream of the shock. One can see that the presence of small-amplitude magnetic field perturbations hardly influences the particle spectrum formation. The spectrum is essentially the superadiabatically compressed initial one, and the power-law part, with a sharp cutoff at $E \sim 10^2 E_0$, is formed by a few particles only. The energetic tail generation is due to locally subluminal magnetic field configurations formed at the shock front, which enable particle reflections or extended interaction with the shock. Since the locally subluminal field configurations are produced mainly by high-amplitude long-wave perturbations, these processes are more efficient for the Kolmogorov-type field perturbations. Therefore, the power-law part of the particle spectrum is flatter in this case, when compared to the spectrum for the flat wave power spectrum. Modifications of the compression process due to the presence of the magnetic field perturbations depend on the shock velocity and on the mean field configuration, as one can see from Figure 5 (see also Ostrowski 1993). For lower $u_{B,1} > 1$, the weakly perturbed magnetic field can modify the spectra, whereas for highly superluminal configurations the power-law part is not generated for $\delta B/B_{0,1} = 0.3$ (Figs. 5*e* and 5*f*). At larger turbulence amplitudes power-law sections in the spectra are again produced in the limited energy ranges. The spectral indices vary with varying conditions at the shock, including the shock velocity, the mean field inclination, and the amplitude and spectrum of magnetic field perturbations. The steepening and the cutoff occur at low energies, in the resonance range, contrary to the subluminal shocks at the same turbulence amplitudes.

The spectrum steepening and the cutoff in the resonance energy range are related to the character of the first-order Fermi process at superluminal shocks, in conditions of a highly perturbed magnetic field near the shock. The presence of three-dimensional, finite-amplitude magnetic field perturbations enables efficient particle cross-field diffusion (e.g., Giacalone & Jokipii 1994) but also leads to the formation of locally oblique, subluminal field configurations at the shock front. Such configurations are formed by long-wave high-amplitude magnetic field perturbations and enable particle interactions with the shock in locally subluminal conditions. In some cases reflections from compressed downstream fields can also occur. In effect, the energy gains of particles interacting with the shock in the locally subluminal conditions can be much larger than those of particles interacting within the locally superluminal field configurations. The role of this factor in forming particle spectra was originally discussed by Ostrowski (1993). For sufficiently high turbulence amplitude, he obtained power-law spectra in a wide energy range because of similar scattering conditions at each particle energy. In our present simulations, because of the limited wavevector range the scattering conditions vary with a particle energy, leading to spectral features that have not been discussed so far. Figure 7 shows a variation of the particle reflection probability with

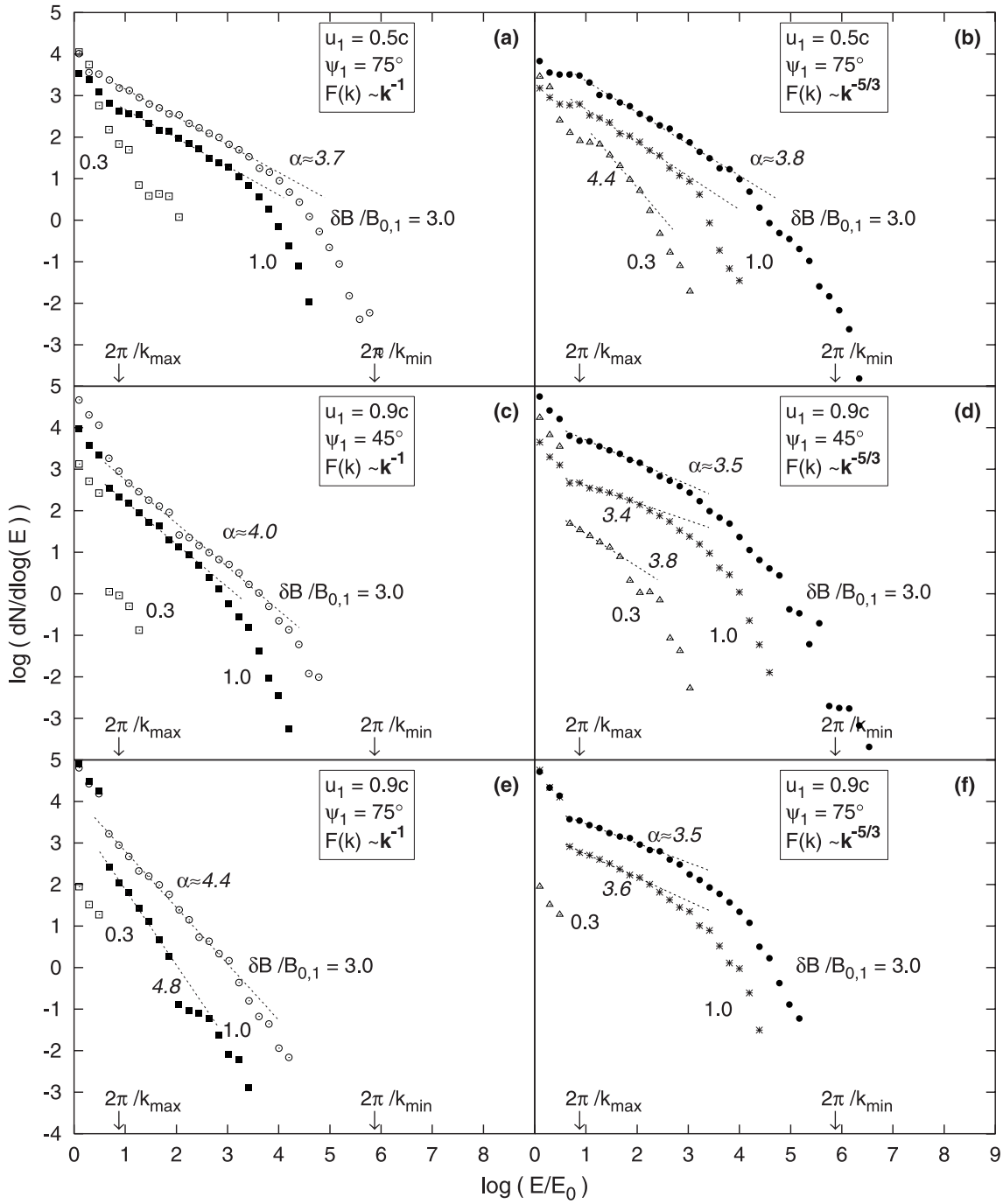


FIG. 5.—Accelerated particle spectra at oblique superluminal shocks with $u_1 = 0.5c$ and $u_1 = 0.9c$. Parameters for each spectrum are provided in the respective panels.

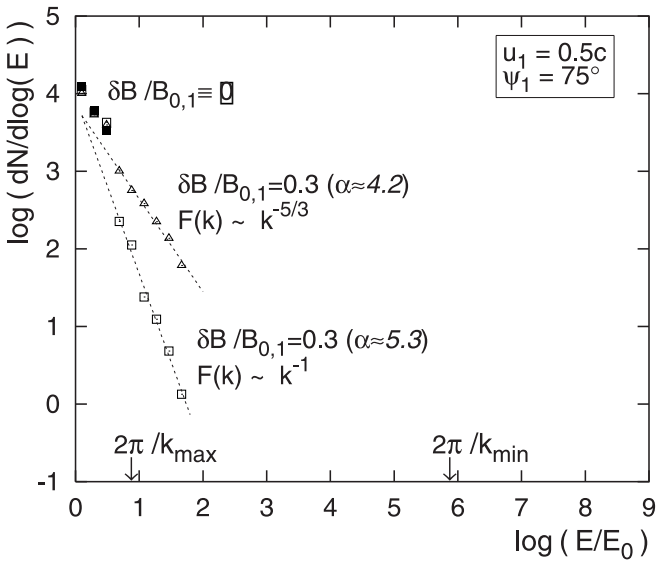


FIG. 6.—Compressed particle spectra at the superluminal shock with $u_{B,1} \simeq 1.93c$. The results for $\delta B/B_{0,1} \equiv 0$ are presented by filled squares. The presence of small-amplitude magnetic field perturbations, $\delta B/B_{0,1} = 0.3$, produces power-law tails, as illustrated by the spectra obtained for the flat (*open squares*) and the Kolmogorov (*open triangles*) wave power spectra. The spectra presented are normalized in such a way as to have the same particle weight in each spectrum.

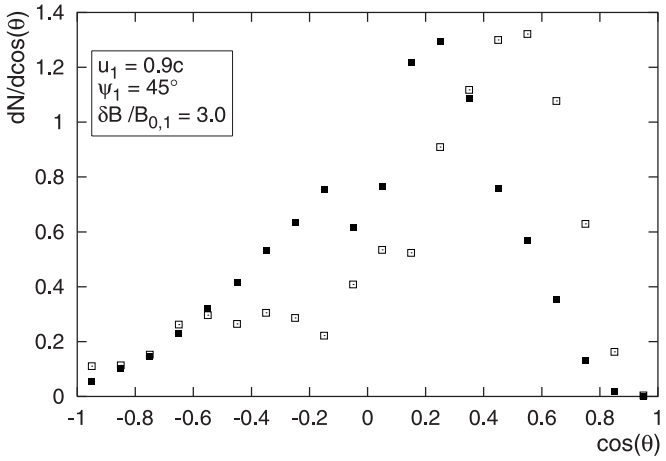


FIG. 8.—Particle angular distributions at the superluminal shock wave for $\delta B/B_{0,1} = 3.0$ in the shock rest frame. The angular distributions are formed by particles with energies in the range $1 \leq \log(E/E_0) \leq 5$ and are shown by the filled and open squares for the Kolmogorov and the flat wave power spectrum, respectively.

the particle energy for the shock wave with $u_1 = 0.9c$ and $\psi_1 = 45^\circ$. We use this parameter to describe subluminal features of the acceleration process. Note, however, that it is not only reflections that are responsible for the observed changes in the acceleration process; variations in the mean energy gain at the particle-shock interaction and in the downstream particle escape rate can also play a role. As shown in Figure 7, in the energy range where a power-law part of the spectrum forms, the reflection probability changes slightly, since particle resonance wavevectors are much larger than $k_{\min}$. Since at a given $\delta B/B_{0,1}$ the amplitudes of long-wave magnetic field perturbations are larger for the Kolmogorov turbulence, P_r is greater in this case. When the reflection probability starts to decrease, the particle spectrum steepens and, finally, for $P_r \simeq 0$, the cutoff occurs. At least two factors can be responsible for the decrease of P_r. The first one is related to the limited dynamic range of the field perturbations: with increasing particle energy there are gradually fewer long waves and most of the particles meet effectively superluminal conditions at the shock. The second

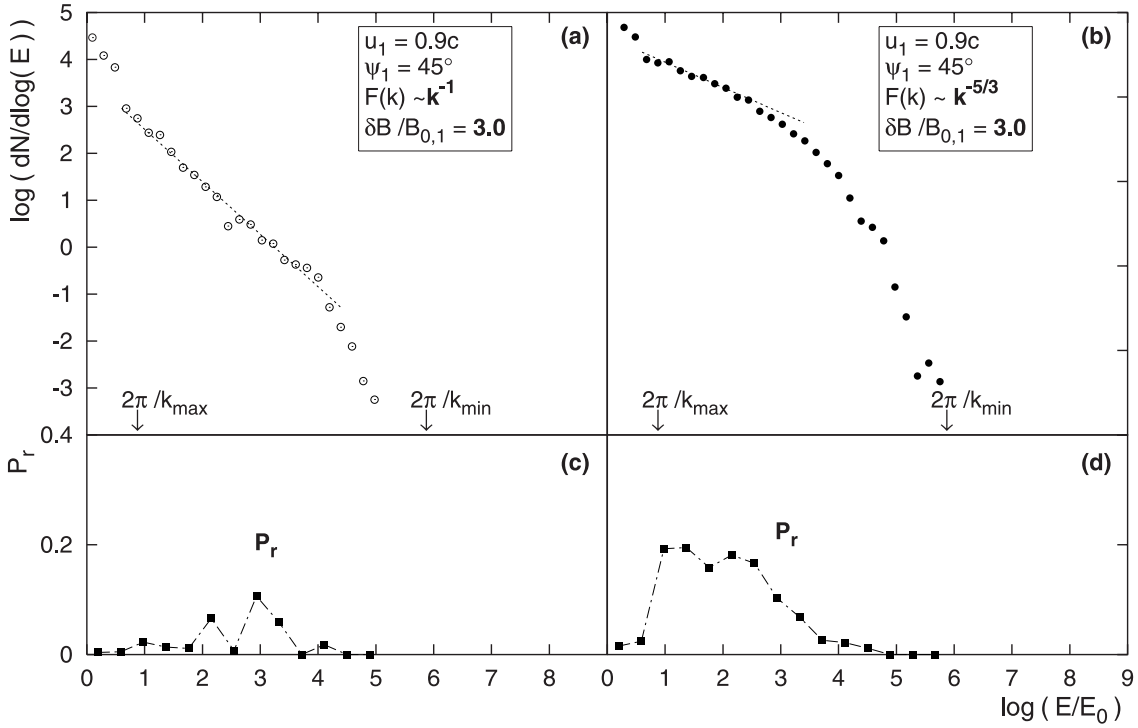


FIG. 7.—Particle spectra at the superluminal shock wave with parameters given in the panels. In the bottom panels the respective particle reflection probability is provided. The spectra presented correspond to those shown in Figs. 5*c* and 5*d* for the case of $\delta B/B_{0,1} = 3.0$.

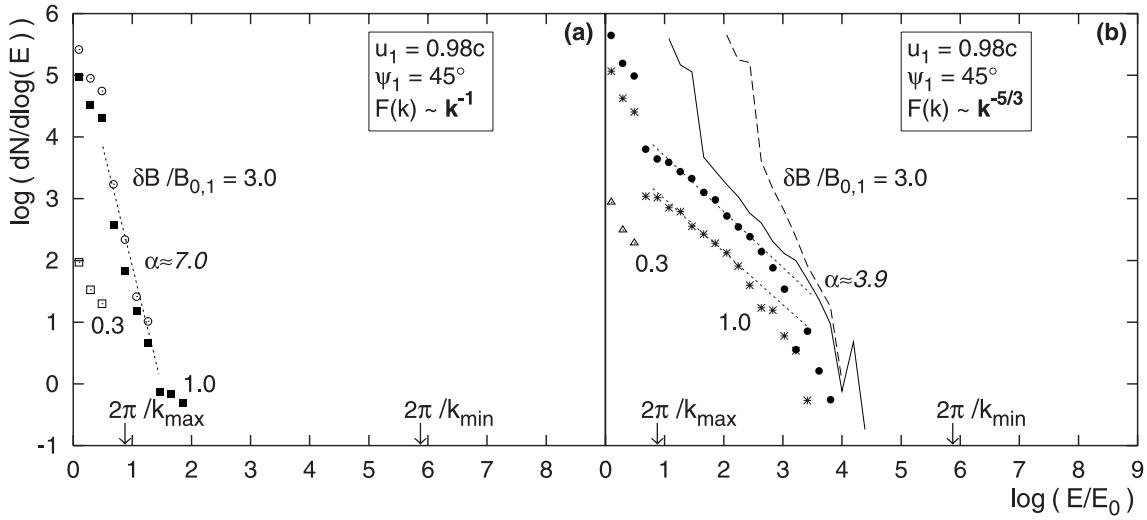


FIG. 9.—Accelerated particle spectra at the ultrarelativistic shock wave ($u_1 = 0.98c$, $\gamma_1 \simeq 5$). In (*b*) the particle spectra obtained for higher particle injection energies $E_{\rm inj}$ are presented by the solid and the dashed lines for $\log(E_{\rm inj}/E_0) = 1$ and $\log(E_{\rm inj}/E_0) = 2$ ($\delta B/B_{0,1} = 3.0$), respectively.

factor is due to the accompanying increase of the resonant perturbation amplitude for the Kolmogorov spectrum, as discussed in § 3.1.

Examples of particle angular distributions derived at the superluminal shock are presented in Figure 8 for the case of the highly perturbed magnetic field $\delta B/B_{0,1} = 3.0$.

3.3. *High-γ Shock Waves*

Particle spectra at the shock wave propagating with velocity $u_1 = 0.98c$ into the magnetic field with the mean field inclined at the angle $\psi_1 = 45^\circ$ are presented in Figure 9. The shock Lorentz factor is $\gamma_1 \simeq 5$, so one can consider the shock an ultrarelativistic one. As can be seen in the figure, the main particle acceleration process in this case is the particle compression at the shock: the power-law tail is formed by only a small fraction of injected particles in the case of a highly perturbed magnetic field. For the flat wave power spectrum the power-law part is very steep, $\alpha \approx 7$; for the Kolmogorov turbulence $\alpha \approx 3.9$ with accuracy $\Delta\alpha \sim 0.1$. The spectrum cutoff occurs well into the resonance energy range, at lower energies in comparison to the lower γ shocks. This feature is independent of the initial energy of particles injected at the shock, as illustrated by the particle spectra calculated for the other injection energies.[6] It seems therefore that it is the turbulent magnetic field structure that becomes effectively perpendicular and does not allow for particle acceleration to higher energies. Note however that the $\gamma_1 \simeq 5$ case we analyzed was at the limit of the application range of our simulation method. Thus this attempt at studying the first-order Fermi process at ultrarelativistic shock waves should be treated with some caution.

3.4. *Parallel Shock Waves*

As discussed by Ostrowski (1988b) for nonrelativistic shocks, the presence of finite-amplitude magnetic field perturbations modifies the character of diffusive particle acceleration at shock waves with the mean field parallel to the shock normal. The effect arises because of locally oblique field configurations formed by long-wave perturbations at the shock front and the respective magnetic field compressions downstream of the shock. As a result, the mean particle energy gains can increase and the particles reflected from the shock front can occur. The analogous phenomena should occur at relativistic shocks (see Ostrowski 1993).

In the numerical simulations of Bednarz & Ostrowski (1996) of the first-order Fermi acceleration at parallel mildly relativistic shocks, the acceleration timescale reduces with increasing turbulence level but no spectral index variation is observed. The same behavior occurs for parallel ultrarelativistic shocks, where the value of the spectral index for a given shock velocity is independent of the magnetic field perturbation amplitude (Bednarz & Ostrowski 1998). However, the considered acceleration models apply very simple modeling of the perturbed magnetic field effects by introducing particle pitch-angle scattering. Such an approach does not allow for studying the effects of long-wave perturbations. We therefore decided to investigate such processes with the "realistic" magnetic field turbulence model applied in the present simulations.

In Figure 10 we present particle spectra for the mildly relativistic parallel shock wave with $u_1 = 0.5c$. The spectral indices fitted to the power-law parts of the spectra are listed in Table 1. One can note that the particle spectral indices deviate from the small-amplitude results of the pitch-angle diffusion model; the values of α calculated by Heavens & Drury (1988) are also presented in the table. In addition, increasing magnetic field perturbations produce nonmonotonic changes in the particle spectral index, the feature that has not been discussed for parallel shocks so far. Analogously to oblique shock waves, our particle spectra are non–power-law ones in a full energy range, and the shape of the spectrum varies with the amplitude of the turbulence and the wave power spectrum.

The nonmonotonic variation of the spectral index with the turbulence amplitude results from modifications of the particle acceleration process at the shock. The long-wave finite-amplitude perturbations produce locally oblique magnetic field configurations and lead to the occurrence of, e.g., particles

[6] The average magnetic field strength $\langle (\boldsymbol{B}_0 + \delta\boldsymbol{B})^2 \rangle^{1/2}$ downstream of the shock is $\langle B_2 \rangle \approx 30 B_{0,1}$ and the wavevectors of magnitude $k_{\rm max}$ are the resonance ones for the particles of energies $E \approx 2\pi \langle B_2 \rangle / k_{\rm max} \approx 18.8$. Simulations for the other injection energies have been performed in order to check whether the cutoff occurring in the particle spectra is not due to the particle injection procedure applied. For the particle injection energy $\log(E/E_0) = 2$ this procedure gives the respective wavevectors $k_{\rm res} = 2\pi / r_g(B = \langle B_2 \rangle) \lesssim k_{\rm max}$ (see § 2.2).

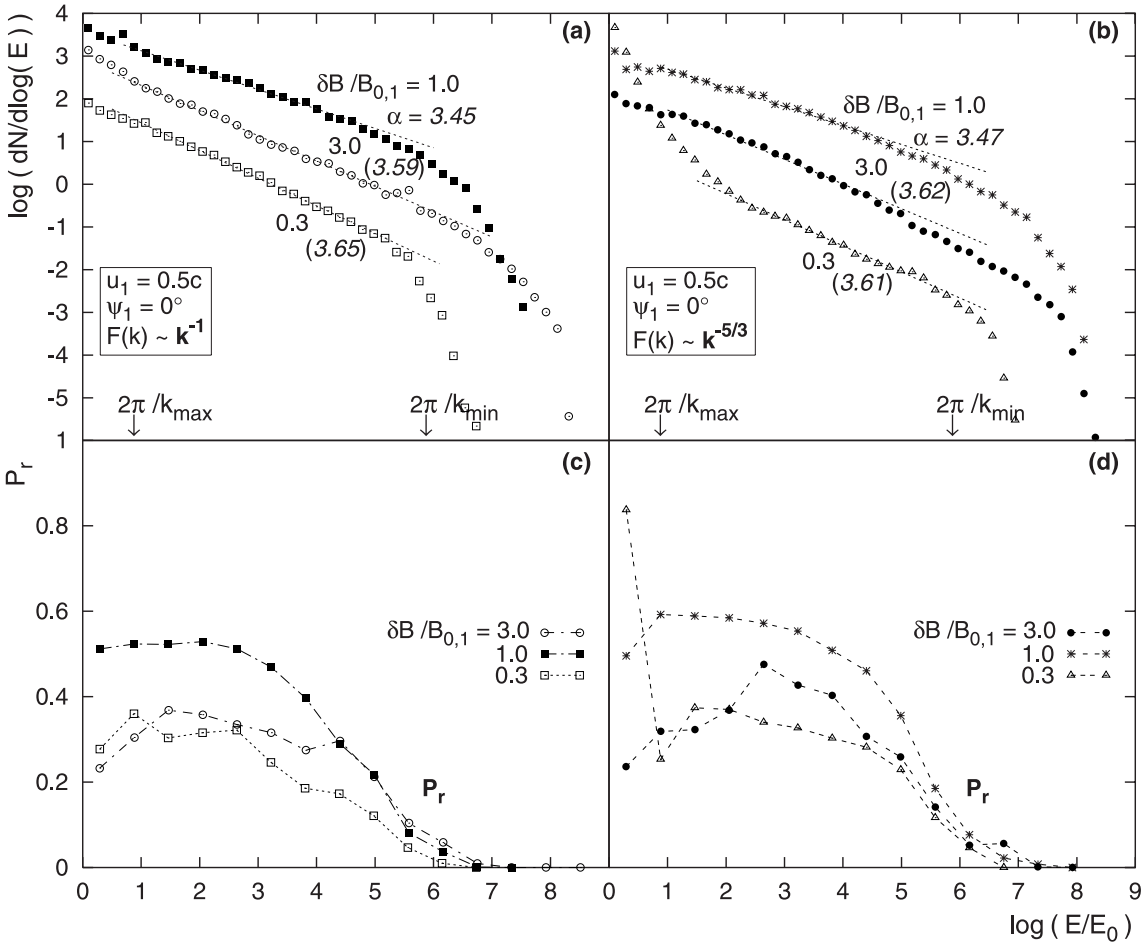


FIG. 10.—Accelerated particle spectra at the parallel shock wave with $u_1 = 0.5c$. For upstream particles, the probability of reflection from the shock, P_r, is presented as a function of a particle energy for the respective particle spectra above.

reflected from the compressed field downstream of the shock. In order to quantitatively estimate effects of such locally oblique field configurations on the particle spectrum formation, we calculated the mean reflection rate and the mean energy gains of particles interacting with the shock. We used the following method (see Ostrowski 1988b). The process of an upstream particle interaction with the shock begins when it crosses the shock front downstream for the first time. A given particle is assumed to continue its interaction with the shock if, after crossing the shock, it reaches the shock front again not later than $1.1t_{g,\max}$ and, at the same time, its distance from the shock does not exceed $2r_{g,\max}$. The particle gyration time $t_{g,\max}$ and the gyroradius $r_{g,\max}$ are derived for the average magnetic field $\langle(\boldsymbol{B}_0 + \delta\boldsymbol{B})^2\rangle^{1/2}$ in the respective local plasma rest frame. A particle trajectory is integrated, including possible successive shock crossings, until it exceeds one of the temporal or spatial barriers thus defined. When it takes place downstream of the shock, the particle is counted as the transmitted one. If it occurs upstream, the particle is assumed to be the reflected one. A reflected particle starts its new interaction when it encounters the shock front again. A transmitted particle, after moving in the perturbed magnetic field, is sometimes able to recross the shock again upstream and to start its new interaction with the shock. For each reflected or transmitted particle, its weight w, final energy E_f, and initial energy E_i are measured, the last quantity derived in the upstream plasma rest frame at the first particle shock crossing. In order to calculate the reflection probability P_r and transmission probability P_{12}, a particle weight is added to the respective logarithmic energy E_i bin for the reflected particles (S_r) and the transmitted ones (S_{12}). Then the reflection probability is calculated as $P_r = S_r/(S_r + S_{12})$ and, analogously, $P_{12} = S_{12}/(S_r + S_{12})$. The particle energy gains are derived as $(E_f - E_i)/E_i$, E_f for the transmitted particles being calculated in the downstream plasma rest frame (see Ostrowski 1988a).

TABLE 1

SPECTRAL INDICES OBTAINED FOR PARALLEL SHOCKS WITH $u_1 = 0.5c$

$\delta B/B_{0,1}$	SPECTRAL INDEX α	
	$q = 0$	$q = 5/3$
$\ll 1$ (analytic)[a]	3.72	3.74
0.3	3.65	3.61
1.0	3.45	3.47
3.0	3.59	3.62

[a] Values of α calculated by Heavens & Drury (1988) for small-amplitude perturbations, $\delta B/B_{0,1} \ll 1$.

Reflection probability as a function of particle energy is presented in Figures 10*c* and 10*d* for the respective particle spectra shown in the top panels. As one can see, the probability of reflection depends on the turbulence amplitude and the amount of field perturbations with wavelengths larger than

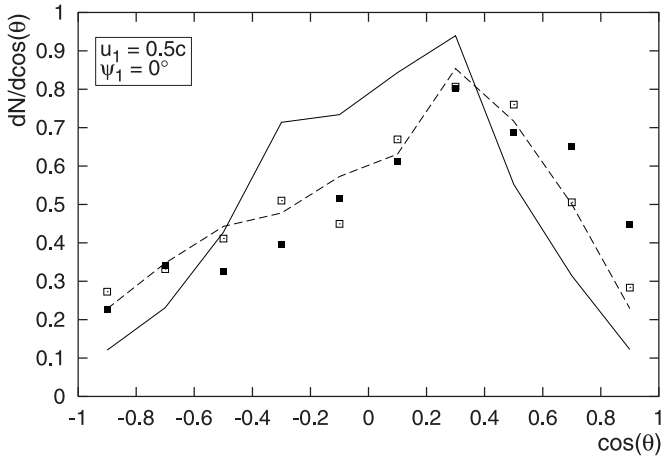


FIG. 11.—Particle angular distributions at the parallel shock wave with $u_1 = 0.5c$ formed by particles with energies in the range $1 \leq \log(E/E_0) \leq 5$ for the small ($\delta B/B_{0,1} = 0.3$; *squares*) and large ($\delta B/B_{0,1} = 3.0$; *lines*) turbulence amplitude. The open squares and dashed line are for $F(k) \sim k^{-1}$; the filled squares and solid line are for $F(k) \sim k^{-5/3}$.

the resonance wavelength for a given particle. For $\delta B/B_{0,1} = 1.0$ the reflection probability is higher as compared to the other perturbation amplitudes considered, and the resulting particle spectrum is flatter. For our chosen $\delta B/B_{0,1} = 0.3$ and 3.0, the values of P_r (and $P_{12} = 1 - P_r$) do not differ considerably, which results in similar particle spectral indices. One can see that the spectra obtained for the Kolmogorov case seem to exhibit a continuous slow steepening. Thus, the fitted power laws depend to some extent on the energy range chosen for the fit, with accompanying variations of α reaching $\Delta\alpha \sim 0.04$. One can also see a steep part of the spectrum at low energies for $\delta B/B_{0,1} = 0.3$ in Figure 10*b*. This is due to weak resonant scattering of low-energy particles, escaping thus along the magnetic field lines through the upstream free escape boundary, located $30{,}000 r_g$ from the shock.

The presented reflection probabilities decrease at high particle energies because of the limited dynamic range of the magnetic field turbulence. The locally oblique field configurations are mainly formed by long-wave perturbations ($k \ll k_{\rm res}$; see Ostrowski 1988b). For high-energy particles with $k_{\rm res} < k_{\rm min}$ there are no such long waves and the upstream particles can be only transmitted downstream of the shock. In these conditions, the acceleration process should converge to the "classic" parallel shock acceleration model, but in our simulations particles can move far from the shock to the introduced escape boundary at $x_{\rm max} = 120 r_g(E)$, forming a cutoff.

Figure 11 shows particle angular distributions for particles forming power-law parts of the energy spectra. For the small amplitude of magnetic field perturbations, $\delta B/B_{0,1} = 0.3$, the derived distributions approximately correspond to those obtained by Heavens & Drury (1988). The presence of large-amplitude perturbations ($\delta B/B_{0,1} = 3.0$) has a noticeable effect on the angular distributions, in comparison to the $\delta B/B_{0,1} = 0.3$ case, only for the Kolmogorov turbulence spectrum.

4. SUMMARY AND FINAL REMARKS

The present work is intended to study the first-order Fermi acceleration processes acting at relativistic shocks. To derive the stationary particle spectra, we apply the test particle approach and neglect the possibility of radiative losses or of the second-order acceleration process acting in the turbulent medium near the shock. The hybrid method applied for a particle trajectory integration allows us to include essential characteristics of particle motion important for the acceleration process. In comparison to previous work, we include a few "realistic" features of the magnetic field turbulence. The field perturbations are imposed on the homogenous component, which allows us to analyze conditions with different mean magnetic field inclinations to the shock normal and a range of turbulence amplitudes. We use an analytic model for the perturbations, forming the power-law spectrum within a wide wavevector range. The turbulent magnetic field is continuous across the shock; the downstream field is derived from the upstream one with the respective shock jump conditions.

The modeling shows how the resulting spectra of accelerated particles depend on the shock velocity and the turbulent magnetic field structure considered. In particular, we demonstrate the effects of the finite wavevector range of the turbulence, leading to deviations of the derived spectra from the usually considered power-law form (e.g., a harder spectral component occurring at high particle energies in subluminal shocks, the spectrum steepening and the formation of the cutoff in the resonance energy range in superluminal shocks). Furthermore, we discuss the role of the long-wave magnetic field perturbations in forming particle spectra. We show that the formation of locally subluminal configurations is important for a power-law spectrum generation at superluminal shocks, but long-wave field perturbations lead to significant modifications of the diffusive acceleration process at parallel shocks as well. In our modeling, we reproduce also a number of previously obtained results. In particular, we demonstrate that particle spectral indices depend on the mean magnetic field configuration and on the amplitude and the wave power spectrum of field perturbations. A strong dependence of test particle spectra on conditions at relativistic shock fronts means that reliable theoretical modeling of real astrophysical sources in which such waves occur can be difficult.

The first-order Fermi process can be applied to sufficiently energetic particles only, which have their gyroradii much larger than the dissipative thickness of the shock, defined possibly by gyroradii of thermal ions present in the plasma. The results of the present paper are valid for such high-energy particles. Particles of lower energies are expected to be accelerated by different processes, such as those discussed by, e.g., Hoshino et al. (1992) or Pohl et al. (2002).

In the present study the particle radiation and other energy losses have been neglected. The role of losses in each particular object can be estimated from comparison of particle acceleration timescales at the shock and the respective timescales for radiation losses downstream of the shock. Since at relativistic shock waves the particle acceleration timescale depends strongly on the shock parameters (Bednarz & Ostrowski 1996) and the background conditions can vary substantially between various objects, such an analysis is not straightforward and requires an independent simulation for each object studied. Qualitatively, if the loss mechanism is synchrotron radiation or inverse Compton scattering, the cutoff in the spectrum at the shock should appear at high particle energy (see Kirk & Schneider 1987b). Downstream of the shock, such a spectrum evolves with the distance from the shock front, and a proper modeling of the spectrum requires again a detailed knowledge of the physical parameters near the shock.

Further progress in the study of relativistic shock particle acceleration is impossible without an understanding of the

microphysics of relativistic shocks. A noticeable advance in this field may result from application of particle-in-cell simulations, which allow for consistent studies of the shock structure, particle injection, and magnetic field generation at the shock (e.g., Drury et al. 2001; Schmitz et al. 2002; Nishikawa et al. 2003; Frederiksen et al. 2003, 2004). Realistic modeling of particle acceleration at relativistic astrophysical shocks, which have to incorporate results of such studies, requires a full plasma nonlinear description. This should take into account appropriate boundary conditions, the second-order acceleration processes, the accelerated particle influence on the shock wave structure (including the possibility of the existence of a cosmic-ray precursor), and the magnetic field turbulence structure in the vicinity of the shock. Monte Carlo numerical simulations have recently been used to study nonlinear particle acceleration at shocks modified by the back-reaction of accelerated particles (Ellison & Double 2002). Estimates of the effectiveness of second-order Fermi process acting in a strongly turbulent field downstream of the shock made by Dermer (2001) suggest that this process is able to produce high-energy particles. To make such models more realistic, there is a need for detailed studies of the problem of magnetic field generation and turbulence evolution near/at the shock.

Let us also stress that the issue of MHD turbulence generation at the shock is of great importance for ultrarelativistic shocks. Such shock waves are suggested to be the gamma-ray burst sources and may also produce ultra–high-energy cosmic rays. Modeling of the burst afterglow spectra often yields results pointing to the asymptotic spectral index $\alpha \approx 4.3$ ($\sigma \approx 2.3$) for radiating electrons, which is sometimes interpreted as observational confirmation of the correctness of theoretical models proposed for ultrarelativistic shock acceleration. As mentioned in § 1, these models consider highly turbulent conditions near the shock. Standard hydrodynamic gamma-ray burst models assume the magnetic field to be generated locally at the ultrarelativistic shock (e.g., Medvedev & Loeb 1999; Nishikawa et al. 2003; Frederiksen et al. 2003, 2004), but the effectiveness of the generation mechanism and the resulting perturbation spectrum is uncertain (but see Frederiksen et al. 2004). If this effectiveness is low, the particle spectra produced at high-γ shocks are expected to be much steeper than the asymptotic ones (see Bednarz & Ostrowski 1998 and also the results of our simulations for $u_1 = 0.98c$), suggesting possibly a different mechanism for particle acceleration (e.g., simplified modeling of electron acceleration by Hoshino et al. 1992, and later particle-in-cell simulations). Therefore, the magnetic field turbulence generation problem has to be analyzed in detail to make realistic estimates of the importance of the first-order Fermi process on the observed parameters of gamma-ray bursts. Generation of ultra–high-energy cosmic rays at such shocks requires the respective long-wave field perturbations too. It is highly uncertain whether such processes take place.

We have performed our modeling in conditions defined in units of a particle gyroradius and a mean inclination of the magnetic field. The respective scaling of these conditions by choosing values for $B_{0,1}$, ψ_1, and the turbulence spectrum allows us, at least formally, to apply these results to various astrophysical objects, as long as losses are unimportant. For situations with radiative processes playing a role, one should repeat the simulations for given physical values of the model parameters and the respective radiative-loss terms.

The work was supported by the Polish State Committee for Scientific Research in 2002–2004 as research project 2 P03D 008 23 (J. N.) and in 2002–2005 as research project PBZ-KBN-054/P03/2001 (M. O.).

APPENDIX A

SHORT WAVES IN OUR HYBRID APPROACH

The influence of short waves ($\lambda \ll r_g$) on particle trajectories is treated here as random, small-amplitude angular perturbations of particle momenta with a discrete scattering procedure described, e.g., by Ostrowski (1991). In this procedure, a particle momentum direction is perturbed at discrete instants of time by a small angle $\Delta\Omega$. Fitting of this approach to the magnetic field turbulence spectrum considered and varying particle energies requires determination of the scattering probability distribution for $\Delta\Omega$. This is determined by the additional simulations described below.

Short waves are defined as the ones with $\lambda < \lambda_{\min} = 0.05 r_g(B = B_{0,1})$. In analogy to the approach described by Ostrowski (1991), in our simulations particle trajectory perturbations are introduced along the "exact" orbit in the magnetic field composed of the mean field and turbulent fluctuations with wavelengths larger than $\lambda_{\min}$. Particle momentum direction perturbations are performed at discrete instants of time separated by Δt. In the present simulations, $\Delta t = 0.01 t_g$ [$t_g = 2\pi r_g(B = B_{0,1})/c$]. At each scattering, the value of the scattering amplitude $\Delta\Omega$ is selected at random from the scattering probability distribution. Since $\Delta\Omega$ stands only for the angular distance between the original and the scattered momentum vectors on the sphere of $|\boldsymbol{p}| = \text{const}$, one also has to specify the scattering azimuthal angle in order to derive the scattered vector orientation. The scattering azimuthal angle is randomly chosen from the range $[0,\ 2\pi]$.

In the additional simulations determining the scattering probability distribution, a large number of particles (usually $N = 10^4$) were injected at random positions and random momentum vector orientations into the turbulent magnetic field composed of the short waves only. The trajectory of each particle was subsequently integrated over the time Δt when the scattering angle $\Delta\Omega$ was derived and the particle weight ($w = 1$) was added to the respective $\log \Delta\Omega$ bin. The scattering probability distribution obtained was ultimately normalized to unity. Because of particle interactions with small-scale field fluctuations, particle spatial positions diverge from the exact trajectory in the magnetic field composed of the mean field and long waves. The shifts introduced are small, however, and we neglect them in order to simplify the scattering model (there are no spatial scatterings accompanying the angular ones). Since the downstream magnetic field structure is different from the upstream one, the scattering probability distribution was determined independently in this region. We emphasize that the probability distribution for $\Delta\Omega$ is not model-assumed (see Kirk & Schneider 1987b; Ostrowski 1991) but is determined by a particular pattern of short waves present in the simulations.

In the wavevector range of the magnetic field perturbations considered, the condition for the short-wave fluctuations [$\lambda < \lambda_{\min}(E)$] is fulfilled by different sets of waves for different particle energies. The scattering conditions and, consequently, the

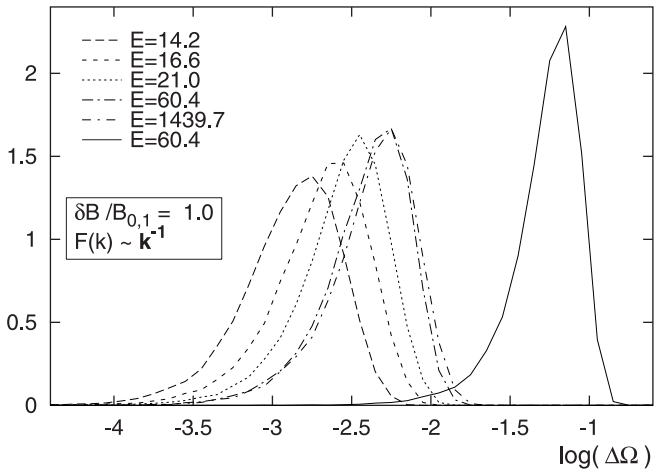


FIG. 12.—Angular scattering probability distributions for selected particle energies for the upstream turbulence amplitude $\delta B/B_{0,1} = 1.0$ and the flat wave power spectrum. The solid line represents distribution of the full turbulent magnetic field influence on particle motion at the same time intervals. All distributions are normalized to unity.

scattering probability distribution vary continuously with particle energy. In our simulations, we calculate these probability distributions for a discrete set of energies. Since our turbulent field is modeled by a discrete wave power spectrum, the consecutive energies are selected in such a way that corresponding short-wave turbulent fields differ by a few waves only. In effect, each subsequent distribution differs modestly from the previous one. Example scattering probability distributions are presented in Figure 12 for the upstream field with $\delta B/B_{0,1} = 1.0$ and the flat wave power spectrum. The mean scattering angle due to short-wave perturbations increases with a particle energy, but it is small in comparison with the full (including all waves) magnetic field influence on particle motion, represented in the figure by the solid line for the selected $E = 60.4$.

In Figure 12 the probability distributions corresponding to highest energies overlap, which indicates similar scattering conditions at these energies. In fact, the most efficient scattering is provided by the long-wavelength part of the short waves considered at any given particle energy, whereas the smallest scales do not contribute significantly to trajectory perturbations. In the turbulent magnetic field with the flat wave power spectrum, the field energy in the waves responsible for scattering is similar for higher energy particles, which results in statistically identical scattering probability distributions in a wide energy range. This is not the case for the Kolmogorov wave spectrum, where the scattering conditions vary with particle energy, leading to variations of the scattering probability distribution, as shown in Figure 13. As one can see, the mean perturbation angle increases continuously with particle energy in this case. Finally, for the highest particle energies all the waves form the small-scale turbulence and the mean perturbation angle starts to decrease.

APPENDIX B

TESTS OF THE SIMULATION METHOD

The Runge-Kutta routine we use for trajectory integration is accurate to fifth order. The embedded fourth-order formula estimates the truncation error at a given point of a particle orbit, which allows for an appropriate step size adjustment to ensure

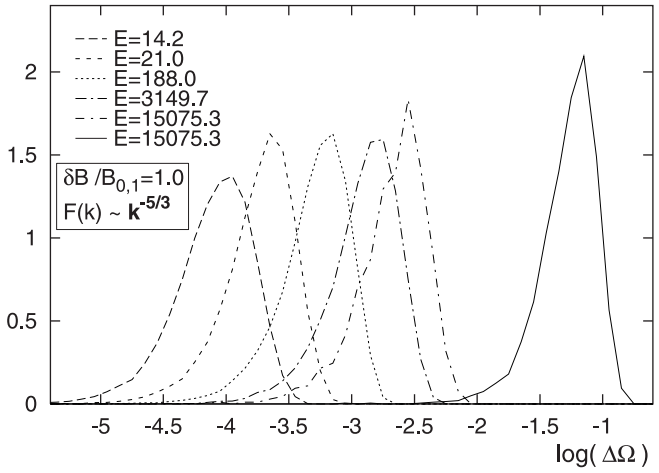


FIG. 13.—Angular scattering probability distributions for the upstream field with $\delta B/B_{0,1} = 1.0$ and the Kolmogorov wave power spectrum. The full magnetic field influence is represented by the solid line.

integration with the accuracy required. We have set the truncation error at every integration step to be less than 10^{-7}. The accuracy imposed allows for a precise and efficient trajectory calculation. With this choice, the particle energy between shock crossings is conserved to better than one part in 10^7. Integration with small but still finite accuracy produces inevitably numerical noise, which influences the stability of calculated trajectories. This noise can be regarded as resulting from an additional small-scale magnetic field turbulence. We have checked, via diffusion coefficient derivations (see Ostrowski 1993), that the energy density in these fluctuations is small and does not change noticeably the wave power spectrum assumed for the simulations. Our trajectories are stable over at least several particle gyroperiods. In the vicinity of a relativistic shock wave, very few particles that form the spectrum stay on either side of the shock front for many gyroperiods between successive shock crossings. The exception may be particles of energy near the injection energy E_0, which only weakly interact with the turbulent field. However, the part of the spectrum formed by these particles is already influenced by the initial conditions.

In order to check whether the method of particle spectra and angular distribution measurement works properly, additional simulations were performed. An isotropic particle source was located at some point in the plasma. On both sides of that point a set of five parallel barriers was placed, each one several particle gyroradii away from every other. Trajectories of $N = 1000$ particles originated at the particle source were subsequently calculated. Every time a particle crossed one of the barriers, a quantity $1/(|v_x| + 0.005)$ was added to the respective $\cos(\theta)$ bins, where θ is the angle between the particle momentum and the normal to a given barrier. Trajectory calculations were finished when a particle escaped far from the external barriers. The resulting particle angular distribution, averaged over 10 different sets of particles and realizations of the turbulent magnetic field, was isotropic, as expected. Small departures from isotropy due to statistical errors occurred only near $\cos\theta \approx 0$, so angular distributions presented in § 3 might be measured with worse quality near that value of $\cos\theta$. These simulations were performed for the upstream turbulent magnetic field with $\delta B/B_{0,1} = 1.0$ and the flat wave power spectrum.

In our hybrid approach, used for particle trajectory integration, the short waves, both upstream and downstream of the shock, are defined by a particle gyroradius in the *upstream* mean magnetic field [$\lambda < \lambda_{\min} = 0.05 r_g(B = B_{0,1})$]. However, in cases of higher turbulence amplitudes, the average magnetic field can be much higher then $B_{0,1}$, especially downstream of the shock, where the magnetic field is amplified by compression. Particle gyroradii are then respectively smaller than $r_g(B = B_{0,1})$. In effect, some part of the resonance wavevectors for a particle of a given energy is treated in the simulations as a short-wave turbulence whose influence on particle trajectories is modeled by the scattering terms. In order to check that the definition of short waves used in our simulations does not generate false results, additional simulations were done with the modified definitions of short-wave perturbations. We have checked all the spectra presented in the paper for the upstream turbulence amplitude $\delta B/B_{0,1} = 3.0$. For this perturbation amplitude, the average upstream magnetic field is equal to $\langle B_1 \rangle \approx 2.3$, and the definition of short waves that we adopted is $\lambda < \lambda_{\min} = 0.02 r_g(B = B_{0,1})$ in this case. The average magnetic field value downstream of the shock depends on the mean field configuration and the compression factor r. For parallel shocks propagating with velocity $u_1 = 0.5c$, $\langle B_2 \rangle \approx 10$ and the definition of short waves is $\lambda < \lambda_{\min} = 0.005 r_g(B = B_{0,1})$. For the above definitions of the short-wave turbulence, the scattering probability distributions have been determined. The particle spectra obtained in the test simulations with the modified definition of short waves are, in the limit of statistical accuracy, the same as those calculated in the simulations with the unmodified definition of small-scale perturbations.[7]

The most important test concerns the hybrid approach we use in the simulations. A straightforward way to check whether it gives correct results would be to perform simulations by integrating exact particle trajectories in the magnetic field with all the turbulence scales present, without introducing the scattering terms. However, it was impossible to perform such modeling with the full range of wavevectors considered ($k_{\max}/k_{\min} = 10^5$) because of the excessive simulation time required. In this situation, we have performed such simulations for a limited wavevector range, with $k_{\min} = 0.01$ and $k_{\max} = 10$. We have investigated the acceleration process at the shock wave moving with velocity $u_1 = 0.5c$, the mean upstream magnetic field inclined at an angle $\psi_1 = 45^\circ$ to the shock normal, and the amplitude of the field turbulence $\delta B/B_{0,1} = 1.0$ with the flat wave power spectrum. In addition, parallel simulations were performed with the use of the original hybrid approach, with the same simulation parameters. Both methods yielded the same results within the statistical accuracy: the particle spectrum is a power-law in a finite energy range, followed by the harder component. Statistical accuracy of the spectral index calculation for the modeling without scattering terms was here rather low, because these simulations have been performed for only one set of $N = 100$ injected particles and one realization of the turbulent magnetic field.

[7] The value of the average downstream magnetic field can be larger for faster shocks (e.g., for $u_1 = 0.9c$, $\psi_1 = 45^\circ$, $\langle B_2 \rangle \approx 16$), so the required $\lambda_{\min}$ should be respectively smaller. However, for such small $\lambda_{\min}$ the simulation time would be very long.

REFERENCES

Achterberg, A., Gallant, Y. A., Kirk, J. G., & Guthmann, A. W. 2001, MNRAS, 328, 393
Ballard, K. R., & Heavens, A. 1992, MNRAS, 259, 89
Bednarz, J., & Ostrowski, M. 1996, MNRAS, 283, 447
———. 1998, Phys. Rev. Lett., 80, 3911
Begelman, M. C., & Kirk, J. G. 1990, ApJ, 353, 66
Boldyrev, S., Nordlund, Å., & Padoan, P. 2002, Phys. Rev. Lett., 89, 031102
Cho, J. 2001, J. Korean Astron. Soc., 34, S275
Cho, J., Lazarian, A., & Vishniac, E. T. 2003, ApJ, 595, 812
Decker, R. B., & Vlahos, L. 1985, J. Geophys. Res., 90, 47
Dermer, C. D. 2001, in Proc. 27th Int. Cosmic Ray Conf. (Hamburg), 2039
Drury, L. O'C. 1983, Rep. Prog. Phys., 46, 973
Drury, L. O'C., McClements, K. G., Chapman, S. C., Dendy, R. O., Dieckmann, M. E., Lyung, P., & Ynnerman, A. 2001, in Proc. 27th Int. Cosmic Ray Conf. (Hamburg), 2096
Ellison, D. C., & Double, G. P. 2002, Astropart. Phys., 18, 213
Ellison, D. C., Jones, F. C., & Reynolds, S. P. 1990, ApJ, 360, 702
Frederiksen, J. T., Hededal, C., Haugbølle, T., & Nordlund, Å. 2003, in Proc. First Niels Bohr Summer Institute on Beaming and Jets in Gamma Ray Bursts (Stanford: Stanford Univ.), http://www.slac.stanford.edu/econf/C0208122/docs/nordlund.pdf
———. 2004, ApJ, 608, L13
Gallant, Y. A., & Achterberg, A. 1999, MNRAS, 305, L6
Gallant, Y. A., Achterberg, A., & Kirk, J. G. 1999, A&AS, 138, 549
Giacalone, J., & Jokipii, J. R. 1994, ApJ, 430, L137

Hammersley, J. M., & Handscomb, D. C. 1965, Monte Carlo Methods (2nd ed.; London: Spottiswoode, Ballantyne & Co. Ltd.)
Heavens, A., & Drury, L. O'C. 1988, MNRAS, 235, 997
Hoshino, M., Arons, J., Gallant, Y. A., & Langdon, A. B. 1992, ApJ, 390, 454
Karimabadi, H., Krauss-Varban, D., & Terasawa, T. 1992, J. Geophys. Res., 97, 13853
Kirk, J. G., Guthmann, A. W., Gallant, Y. A., & Achterberg, A. 2000, ApJ, 542, 235
Kirk, J. G., & Heavens, A. 1989, MNRAS, 239, 995
Kirk, J. G., & Schneider, P. 1987a, ApJ, 315, 425
———. 1987b, ApJ, 322, 256
Lagage, P. O., & Cesarsky, C. J. 1983, A&A, 118, 223
Leamon, R. J., Smith, C. W., Ness, N. F., Matthaeus, W. H., & Wong, H. K. 1998, J. Geophys. Res., 103, 4775
Lee, L. C., & Jokipii, J. R. 1976, ApJ, 206, 735
Lemoine, M., & Pelletier, G. 2003, ApJ, 589, L73
Lucek, S. G., & Bell, A. R. 2000, MNRAS, 314, 65
Medvedev, M. V., & Loeb, A. 1999, ApJ, 526, 697
Naito, T., & Takahara, F. 1995, MNRAS, 275, 1077
Nishikawa, K.-I., Hardee, P., Richardson, G., Preece, R., Sol, H., & Fishman, G. J. 2003, ApJ, 595, 555
Ostrowski, M. 1988a, MNRAS, 233, 257
———. 1988b, A&A, 206, 169
———. 1991, MNRAS, 249, 551
———. 1993, MNRAS, 264, 248
———. 2002, J. Phys. Studies, 6, 393, http://www.ktf.franko.lviv.ua/JPS/2002/4/ps/393_400.ps.gz
Ostrowski, M., & Bednarz, J. 2002, A&A, 394, 1141
Pohl, M., Lerche, R., & Schlickeiser, R. 2002, A&A, 383, 309
Press, W., Teukolsky, S. A., Vetterling, W. T., & Flannery, B. P. 1992, Numerical Recipes in FORTRAN 77 (2nd ed.; Cambridge: Cambridge Univ. Press)
Schmitz, H., Chapman, S. C., & Dendy, R. O. 2002, ApJ, 570, 637
Stinebring, D. R., Smirnova, T. V., Hankins, T. H., Hovis, J. S., Kaspi, V. M., Kempner, J. C., Myers, E., & Nice, D. J. 2000, ApJ, 539, 300
Webb, G. M., Axford, W. I., & Terasawa, T. 1983, ApJ, 270, 537